JCTC Journal of Chemical Theory and Computation

Article

pubs.acs.org/JCTC

First Principles Studies of the Vibrationally Resolved Magnetic Circular Dichroism Spectra of Biphenylene

Na Lin,[†,‡] Harald Solheim,[‡] Xian Zhao,*[,†] Fabrizio Santoro,*[,§] and Kenneth Ruud[‡]

[†]State Key Laboratory of Crystal Materials, Shandong University, 250100 Jinan, Shandong, People's Republic of China

[‡]Centre for Theoretical and Computational Chemistry, Department of Chemistry, University of Tromsø, N-9037 Tromsø, Norway

[§]Consiglio Nazionale delle Ricerche—CNR, Istituto di Chimica dei Composti Organo Metallici (ICCOM-CNR), UOS di Pisa, Area della Ricerca, Via G. Moruzzi 1, I-56124 Pisa, Italy

Supporting Information

ABSTRACT: We present density-functional response theory calculations of the one-photon absorption and magnetic circular dichroism spectral bandshapes of biphenylene. The effects from the surrounding solvent environment and molecular vibrations have been included. The solvent is described by the Polarizable Continuum Model (PCM), while the vibrational structures of the spectra have been computed including both Franck−Condon and Herzberg−Teller contributions in the vibronic model. This is the first study of vibronic effects on magnetic circular dichroism spectra including non-Franck−Condon contributions. A detailed comparison with experimental data has been performed, revealing that the B3LYP functional in combination with PCM gives the best agreement with experimental data. Our calculations indicate that nonadiabatic vibronic coupling may play a role, and even small computational inaccuracies might cause significant changes in the calculated HT term, which raises concerns about the inclusion of HT contributions in the calculations of vibronic MCD in systems that have close-lying excited states.

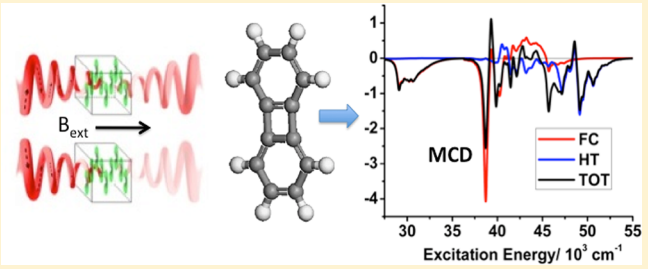

1. INTRODUCTION

The difference between the one-photon absorption of left and right circularly polarized light of chiral molecules is known as natural circular dichroism.[1] However, circular dichroism can be observed for all molecules in the presence of a static magnetic field aligned in the direction of the propagating light. This phenomenon is known as magnetic circular dichroism (MCD). The theory and experimental details of MCD have been the subject of many reviews.[2−6] MCD is a very valuable tool for classifying electronic transitions and has in principle a much larger applicability than natural circular dichroism as it is not limited to chiral systems. MCD is in fact a powerful tool for detecting weak transitions that are either buried under a stronger transition or are too weak to be observed in conventional absorption spectra.[7] MCD is also valuable in exploring orbitally degenerate excited states in molecules,[8] as well as for understanding spin-level populations in open-shell species.

There are in general three different contributions to an observed MCD spectrum arising from different interaction mechanisms between the molecule and the applied magnetic and electromagnetic fields, conventionally referred to as the Faraday A, B, and C terms.[9] The Faraday A term originates from the Zeeman splitting of spectral lines into right- and left-circularly polarized components, which is nonzero only when either the ground and/or the excited states are degenerate. The Faraday C term originates from a change of the electronic population of the magnetically split ground state, and it is nonzero only for open-shell species in which there is a ground-state degeneracy. Therefore, only in molecules with a 3-fold or higher-order rotation axis can the A and C terms be generated. In contrast, all electronic excitations will exhibit B terms in the presence of an external magnetic field due to the field-induced mixing of the energy levels.

In the present study, biphenylene has been chosen as our model system, whose experimental one-photon absorption (OPA) and MCD spectra have been reported and discussed by Michl and co-workers.[10,11] Biphenylene is a closed shell system of D_{2h} symmetry and does not have degenerate electronic states. Therefore, its MCD spectrum is due only to the B term and is moreover naturally gauge invariant according to the symmetry rules derived by Seamans and Moscowitz.[12] Both the OPA and MCD spectra of biphenylene will be studied using density functional response theory.[13,14] The relevant absorption intensities and rotational strengths are obtained as single residues of linear and suitable quadratic response functions,[15] respectively. The effects of the surrounding solvent and molecular vibrations have been taken into account in the calculations in order to allow for a more faithful comparison with experimental data. The interactions between the solute and the solvent will be described by the polarizable continuum

Received: December 17, 2012
Published: January 29, 2013

dx.doi.org/10.1021/ct301101h | J. Chem. Theory Comput. 2013, 9, 1557−1567

model (PCM),[16−20] in which the solute molecule is placed in a cavity in a continuum that describes the solvent. We take into account the molecular vibrations in the framework of the adiabatic approximation,[21,22] which has been shown to be a reliable approximation to the full vibronic problem when the excited states are well separated in energy, which is also the basic assumption in the calculation of MCD B terms from single residues of quadratic response functions.[23]

The remainder of this paper is organized as follows: In section 2, the theoretical methods will be briefly outlined. Computational details follow in section 3. The results of our study are presented and discussed in section 4, and section 5 collects our main conclusions.

2. THEORY

2.1. General Formalism for Vibrationally Resolved OPA Spectra. For OPA, when both electronic and vibrational states are taken into account, the extinction coefficient can be written as[24]

$$\begin{aligned}&\varepsilon_{\mathrm{OPA}}(\omega)\ [\mathrm{L\ mol^{-1}\ cm^{-1}}]\\&= \frac{(2\pi)^2 \times \omega \times N_{\mathrm{A}}}{3 \times 1000 \times \ln(10) \times \hbar c_0 \times (4\pi\varepsilon_0)} \times \sum_f \sum_{\nu_g,\nu_f} p_{\nu_g}\, g(\omega, \omega_{g\nu_g f\nu_f}) \sum_{\alpha=x,y,z} |\mu_\alpha^{g\nu_g f\nu_f}|^2\\&\approx 703.301 \times \omega\ [\mathrm{au}] \times \sum_f \sum_{\nu_g,\nu_f} p_{\nu_g}\, g(\omega, \omega_{g\nu_g f\nu_f})\ [\mathrm{au^{-1}}] \times \sum_{\alpha=x,y,z} |\mu_\alpha^{g\nu_g f\nu_f}|^2\ [\mathrm{au}]\end{aligned} \tag{1}$$

where N_{A} is Avogadro's number, c_0 is the speed of light in vacuo, and ε_0 is the electric constant. ω is the circular frequency of the laser, $\omega_{g\nu_g f\nu_f}$ is the transition energy from the initial state $|g\nu_g\rangle$ to the final state $|f\nu_f\rangle$. Here $|\nu_g\rangle$ and $|\nu_f\rangle$ label the vibrational states associated with the electronic states $|g\rangle$ and $|f\rangle$, respectively. p_{ν_g} is the Boltzmann thermal population of the initial vibrational state $|\nu_g\rangle$. $g(\omega,\omega_{g\nu_g f\nu_f})$ is the line broadening function.

The transition electric dipole moment is evaluated explicitly as

$$\mu_\alpha^{g\nu_g f\nu_f} = \langle g\nu_g|\mu_\alpha|f\nu_f\rangle \tag{2}$$

with μ_α denoting the Cartesian ($\alpha = x,y,z$) component of the electric dipole operator. Applying the Born−Oppenheimer approximation in eq 2, we obtain

$$\mu_\alpha^{g\nu_g f\nu_f} = \langle \nu_g|\mu_\alpha^{e,gf}(\mathbf{Q})|\nu_f\rangle \tag{3}$$

where $\mathbf{Q}$ is the set of normal coordinates and $\mu_\alpha^{e,gf}(\mathbf{Q})$ is the so-called electronic transition dipole moment. The latter can be expanded in a Taylor series with respect to the normal coordinates of the ground electronic state ${}^g\mathbf{Q}$ around the equilibrium geometry ${}^g\mathbf{Q}^0$:

$$\mu_\alpha^{e,gf}({}^g\mathbf{Q}) = \mu_\alpha^{e,gf}({}^g\mathbf{Q}_0) + \sum_i \left(\frac{\partial \mu_\alpha^{e,gf}({}^g\mathbf{Q})}{\partial {}^gQ_i}\right)_{{}^g\mathbf{Q}_0} {}^gQ_i + \ldots \tag{4}$$

Inserting this expansion into eq 3, limiting ourselves to the first two terms, we obtain

$$\mu_\alpha^{e,gf}({}^g\mathbf{Q}) = \mu_\alpha^{e,gf}({}^g\mathbf{Q}^0)\langle \nu_g|\nu_f\rangle + \sum_i \left(\frac{\partial \mu_\alpha^{e,gf}({}^g\mathbf{Q})}{\partial {}^gQ_i}\right)_{{}^g\mathbf{Q}^0} \langle \nu_g|{}^gQ_i|\nu_f\rangle \tag{5}$$

The first quantity on the right-hand side is the electronic transition moment of the initial state at the equilibrium position of the ground electronic state, multiplied by the Franck−Condon (FC) overlap. The second term arises from the vibronic coupling between different electronic states and yields the so-called Herzberg−Teller (HT) contribution.

2.2. General Formalism for Vibrationally Resolved MCD Spectra. The measurement of MCD involves the determination of the decadic extinction coefficient, which depends on the strength of the applied magnetic field, and it is therefore usually given as molar absorptivity per unit magnetic field strength ($\mathrm{L\ mol^{-1}\ cm^{-1}\ T^{-1}}$). For our system, the transitions occur between nondegenerate states, and the only surviving Faraday term is the B term. The MCD extinction coefficient comparable with experimental data can be expressed as[25]

$$\frac{\Delta\varepsilon(\omega)}{B_{\mathrm{ext}}}\ [\mathrm{L\ mol^{-1}\ cm^{-1}\ T^{-1}}] = -5.98442 \times 10^{-3} \times \omega\ [\mathrm{au}] \times \sum_f \sum_{\nu_g,\nu_f} p_{\nu_g}\, g(\omega, \omega_{g\nu_g f\nu_f})\ [\mathrm{au^{-1}}] \times B(g\nu_g \rightarrow f\nu_f)\ [\mathrm{au}] \tag{6}$$

The Faraday B term is given as[3,4]

$$\begin{aligned}&B(g\nu_g \rightarrow f\nu_f)\\&= \varepsilon_{\alpha\beta\gamma}\mathrm{Im}\left[\sum_{k\neq g,\nu_k} \frac{\langle g\nu_g|\mu_\alpha|f\nu_f\rangle\langle f\nu_f|\mu_\beta|k\nu_k\rangle\langle k\nu_k|m_\gamma|g\nu_g\rangle}{\omega_k + \omega_{\nu_k} - \omega_g - \omega_{\nu_g}} + \sum_{k\neq f,\nu_k} \frac{\langle g\nu_g|\mu_\alpha|f\nu_f\rangle\langle f\nu_f|m_\gamma|k\nu_k\rangle\langle k\nu_k|\mu_\beta|g\nu_g\rangle}{\omega_k + \omega_{\nu_k} - \omega_f - \omega_{\nu_f}}\right]\end{aligned} \tag{7}$$

with m_γ denoting the Cartesian ($\gamma = x,y,z$) component of the magnetic dipole operator. Here the summations run over all the intermediate electronic ($|k\rangle$) and vibrational ($|\nu_k\rangle$) states. Direct application of eq 7 is only feasible in cases where the summation over the intermediate states can be limited to a very small number.[26−28] On the other hand, at the purely electronic level of theory, a complete inclusion of all intermediate states, within the approximate description provided by the chosen basis set and correlation description, is now possible using response theory.[13−15] This is important for molecules such as biphenylene which display a large number of low-lying electronic states with none of them leading to dominating resonance contributions. The simplest way to put eq 7 in a suitable form to exploit response theory is to assume that the vibrational energy differences $\omega_{\nu_k} - \omega_{\nu_g}$ are small with respect to $\omega_k - \omega_g$ and therefore can be neglected. In this way, using the closure relation $\sum_{\nu_k}|\nu_k\rangle\langle\nu_k| = 1$, we have

$$B(gv_g \rightarrow fv_f) = \varepsilon_{\alpha\beta\gamma}\mathrm{Im}\langle v_g|\mu_\alpha^{e,gf}(\mathbf{Q})|v_f\rangle\langle v_f|T_{\beta\gamma}^{e,fg}(\mathbf{Q})|v_g\rangle = \varepsilon_{\alpha\beta\gamma}\mathrm{Im}[\mu_\alpha^{gv_gfv_f}T_{\beta\gamma}^{gv_gfv_f,*}] \quad (8)$$

where $T_{\beta\gamma}^{e}(\mathbf{Q})$ is the electronic (vertical-transition) tensor and

$$T_{\beta\gamma}^{e,fg}({}^g\mathbf{Q}) = \sum_{k\neq g}\frac{\langle f|\mu_\beta|k\rangle\langle k|m_\gamma|g\rangle}{\omega_k-\omega_g} + \sum_{k\neq f}\frac{\langle f|m_\gamma|k\rangle\langle k|\mu_\beta|g\rangle}{\omega_k-\omega_f} \quad (9)$$

As for eq 5, we can do a perturbation expansion of the electronic MCD rotational strength with respect to distortions along the normal coordinates

$$T_{\beta\gamma}^{gv_gfv_f} = T_{\beta\gamma}^{e,gf}({}^gQ^0)\langle v_g|v_f\rangle + \sum_i\left(\frac{\partial T_{\beta\gamma}^{e,gf}({}^gQ)}{\partial {}^gQ_i}\right)_{{}^gQ^0}\langle v_g|{}^gQ_i|v_f\rangle \quad (10)$$

Zgierski[29] has pointed out that the assumption that $\omega_{kv_k}-\omega_{gv_g}$ can be approximated by $\omega_k-\omega_g$ can be rather crude if the final and intermediate states mixed by the static magnetic field are close in energy. The inclusion of the first derivatives of the transition tensors in eqs 5 and 10 with respect to the normal coordinates implicitly accounts to first order for both the variation of $\omega_k-\omega_g$ and the Herzberg–Teller vibronic borrowing mechanism.[29]

2.3. Analytical Sum Rules for the Total Intensity. By summing over all final vibrational states, we can obtain analytical total intensities. These are useful for controlling the convergence of the calculations of the spectra for each final state in terms of the ratio between the sum of state-to-state intensities explicitly considered in the computation of the spectrum and the total analytical intensities. Analytical sum rules for the total intensity of OPA and MCD can be derived following the same procedure we adopted for electronic circular dichroism[30] and two-photon circular dichroism.[31] The expression for the analytical total intensity for OPA reads

$$\sum_{v_g,v_f}I_{\mathrm{OPA}}(\omega) = \sum_{\alpha=x,y,z}\sum_{v_g,v_f}p_{v_g}\langle v_g|\mu_\alpha^e({}^gQ)|v_f\rangle\cdot\langle v_f|\mu_\alpha^e({}^gQ)|v_g\rangle = \sum_{\alpha=x,y,z}\sum_{v_g}p_{v_g}\langle v_g|[\mu_\alpha^e({}^gQ)]^2|v_g\rangle = \sum_{\alpha=x,y,z}\sum_{v_g}p_{v_g}\left\langle v_g\middle|\left[\mu_\alpha^e({}^gQ_0) + \sum_i\frac{\partial\mu_\alpha^e}{\partial {}^gQ_i}{}^gQ_i\right]^2\middle|v_g\right\rangle \quad (11)$$

Since the expectation values of the linear term ${}^gQ_a$ vanish, as well as those of the off-diagonal bilinear terms ${}^gQ_i$ and ${}^gQ_j$, leaving in our approximation only the expectation value of ${}^gQ_i^2$, for each final electronic state f, we obtain

$$\sum_{v_g,v_f}I_{\mathrm{OPA}}(\omega) = \sum_{\alpha=x,y,z}\left[(\mu_\alpha^e({}^gQ_0))^2 + \sum_i\sum_{v_g}p_{v_g}\left(\frac{\partial\mu_\alpha^e}{\partial {}^gQ_i}\right)^2\frac{\hbar}{2\omega_i}(2v_{i,g}+1)\right] = I_{\mathrm{OPA}}^{\mathrm{FC}} + I_{\mathrm{OPA}}^{\mathrm{HT}} \quad (12)$$

where $v_{i,g}$ is the quantum number of ground-state mode i in the vibrational state $|v_g\rangle$. Similarly, we can get the expression for the total intensity for MCD as

$$\begin{aligned}\sum_{v_g,v_f}I_{\mathrm{MCD}}(\omega) &= -\varepsilon_{\alpha\beta\gamma}\sum_{v_g,v_f}p_{v_g}\mathcal{I}\langle v_g|\mu_\alpha^e({}^g\mathbf{Q})|v_f\rangle\langle v_f|T_{\beta\gamma}^e({}^g\mathbf{Q})|v_g\rangle\\ &= -\varepsilon_{\alpha\beta\gamma}\sum_{v_g}p_{v_g}\mathcal{I}\langle v_g|\mu_\alpha^e({}^g\mathbf{Q})T_{\beta\gamma}^e({}^g\mathbf{Q})|v_g\rangle\\ &= -\varepsilon_{\alpha\beta\gamma}\sum_{v_g}p_{v_g}\mathcal{I}\left\langle v_g\middle|\left\{[\mu_\alpha^e({}^g\mathbf{Q}_0) + \sum_i\frac{\partial\mu_\alpha^e}{\partial {}^gQ_i}{}^gQ_i][T_{\beta\gamma}^e({}^g\mathbf{Q}_0) + \sum_j\frac{\partial T_{\beta\gamma}^e}{\partial {}^gQ_j}{}^gQ_j]\right\}\middle|v_g\right\rangle\end{aligned} \quad (13)$$

Analogously to what was obtained for OPA, for MCD only the expectation values of ${}^gQ_i^2$ contribute to the analytical sum and for each final electronic state f we obtain

$$\sum_{v_g,v_f}I_{\mathrm{MCD}}(\omega) = -\varepsilon_{\alpha\beta\gamma}\mathcal{I}\left[\mu_\alpha^e({}^g\mathbf{Q}_0)T_{\beta\gamma}^e({}^g\mathbf{Q}_0) + \sum_a\sum_{v_g}p_{v_g}\frac{\partial\mu_\alpha^e}{\partial {}^gQ_a}\frac{\partial T_{\beta\gamma}^e}{\partial {}^gQ_a}\frac{\hbar}{2\omega_a}(2v_{a,g}+1)\right] = I_{\mathrm{MCD}}^{\mathrm{FC}} + I_{\mathrm{MCD}}^{\mathrm{HT}} \quad (14)$$

2.4. Vertical Gradient Model. The vertical gradient (VG) vibronic model assumes that the excited and ground electronic states have the same harmonic potential energy surface (PES) curvatures (that is, the molecular Hessian is the same) and that these PESs only differ by small displacements along the directions of the normal coordinates that can be simply derived from a knowledge of the excited-state PES gradients.[59] We refer interested readers to refs 32–34 for a detailed description of the VG model. This model has been implemented in *FCClasses*,[35] the code which has been used in the present work. The VG model avoids the often cumbersome optimization of excited-state geometries and has been proven to provide a simple approximation to the full vibronic problem that is capable of capturing the most important features of the vibrational structures of one- and two-photon absorption and emission spectra in many cases.[32−34,36−39] We will here test its applicability in the study of vibronic features of MCD spectra. It is noteworthy that vibrationally resolved spectra have been computed also for other chiroptical spectroscopies, like circularly polarized luminescence (CPL),[40] with the same code[35] here adopted, and that it has been shown that

dx.doi.org/10.1021/ct301101h | J. Chem. Theory Comput. 2013, 9, 1557−1567

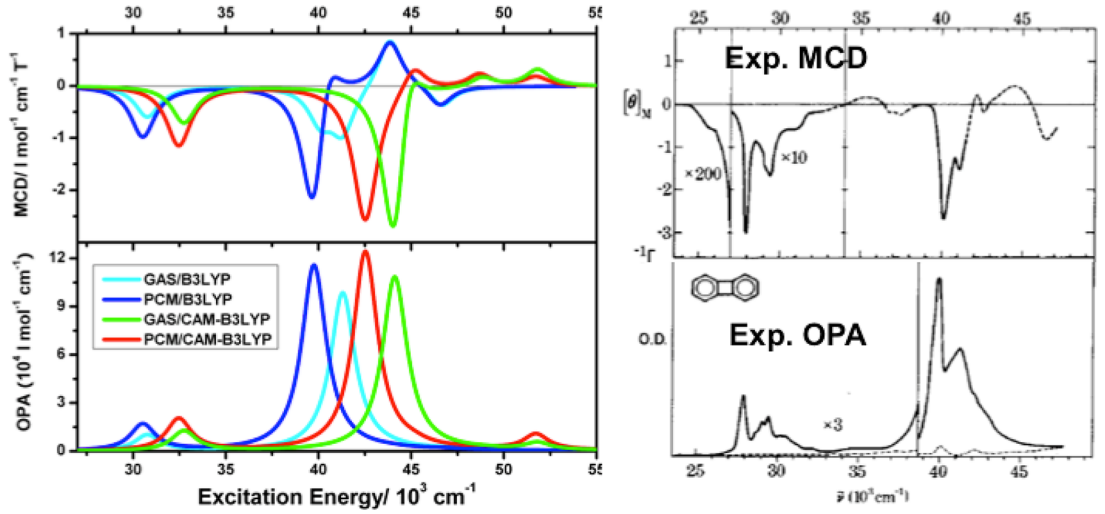

Figure 1. The OPA (left, bottom panel) and MCD (left, top panel) spectra of biphenylene calculated at the B3LYP/aug-cc-pVDZ and CAM-B3LYP/aug-cc-pVDZ levels of theory both in the gas phase and in cyclohexane. A Lorentzian line width of 0.1 eV was employed for the convolution. The corresponding experimental spectra, reprinted with permission from ref [11], are shown in the right panels.

Table 1. Vertical Excitation Energy E^e_{gf} (eV), Vertical One-Photon Absorption Intensity Reported as $I_{OPA} = |\mu^e_\alpha|^2$ (au), and Vertical Magnetic-Circular Dichroism Intensity Reported as $I_{MCD} = -\epsilon_{\alpha\beta\gamma}\,\mathrm{Im}[\mu^e_\alpha T^e_{\beta\gamma}{}^*]$ (au) for Each of the 16 Lowest Excited States of Biphenylene, Calculated at Both the B3LYP/aug-cc-pVDZ and CAM-B3LYP/aug-cc-pVDZ Levels of Theory, Both in the Gas Phase and in Cyclohexane

	GAS/B3LYP			GAS/CAM-B3LYP			PCM/B3LYP			PCM/CAM-B3LYP		
state	E^e_{gf}	I_{OPA}	I_{MCD}	E^e_{gf}	I_{OPA}	I_{MCD}	E^e_{gf}	I_{OPA}	I_{MCD}	E^e_{gf}	I_{OPA}	I_{MCD}
S1	3.25	0.0000	0.0000	3.48	0.0000	0.0000	3.24	0.0000	0.0000	3.47	0.0000	0.0000
S2	3.82	1.1590	−8.1408	4.06	1.3690	−9.0827	3.79	1.9512	−13.4449	4.03	2.2171	−14.8074
S3	4.76	0.0000	0.0000	5.22	0.0000	0.0000	4.77	0.0000	0.0000	5.21	0.0000	0.0000
S4	4.98	0.0759	−6.6948	5.35	0.0000	0.0000	4.93	10.4233	−30.9804	5.28	10.4994	−25.8808
S5	5.09	0.0000	0.0000	5.47	8.7854	−33.5514	5.02	0.0944	15.0135	5.35	0.0000	0.0000
S6	5.13	8.5580	−8.8123	5.56	0.1012	14.6877	5.08	0.0000	0.0000	5.60	0.1279	4.9142
S7	5.15	0.0000	0.0000	5.69	0.0000	0.0000	5.20	0.0000	0.0000	5.74	0.0000	0.0000
S8	5.37	0.0000	0.0000	5.85	0.0000	0.0000	5.33	0.0000	0.0000	5.78	0.0000	0.0000
S9	5.44	0.0162	9.6457	6.02	0.0000	0.0000	5.44	0.0282	8.6891	6.04	0.0483	2.2000
S10	5.48	0.0000	0.0000	6.10	0.0175	1.7215	5.52	0.0000	0.0000	6.06	0.0000	0.0000
S11	5.53	0.0000	0.0000	6.15	0.0000	0.0000	5.59	0.0000	0.0000	6.20	0.0000	0.0000
S12	5.79	0.0296	−3.7474	6.40	0.0000	0.0000	5.77	0.0411	−3.7750	6.41	0.0000	0.0000
S13	5.87	0.0000	0.0000	6.49	0.0000	0.0000	5.86	0.0000	0.0000	6.42	0.6748	1.5201
S14	5.99	0.0000	0.0000	6.60	0.3080	2.6769	6.00	0.0000	0.0000	6.50	0.0000	0.0000
S15	6.02	0.0000	0.0000	6.63	0.0000	0.0000	6.01	0.0000	0.0000	6.55	0.0000	0.0000
S16	6.04	0.0000	0.0000	6.65	0.0000	0.0000	6.08	0.0000	0.0000	6.68	0.0000	0.0000

vibrational corrections can have remarkable effects on magneto-optical rotation.[41]

3. COMPUTATIONAL DETAILS

In this paper, the vibronically resolved OPA and MCD spectra are obtained from a consideration of the first 16 excited electronic states, S1 to S16, of biphenylene. Geometry optimization, as well as the calculation of the vibrational normal modes of the electronic ground state, was carried out using Gaussian 09[42] at the DFT level of theory, based on the hybrid Becke three-parameter exchange functional[43,44] and the Lee−Yang−Parr correlation functional,[45] denoted as the B3LYP functional.[46,47] The geometry reoptimization with PCM simulating the experimental cyclohexane solvation environment yielded no changes. We computed the OPA and MCD spectroscopic properties, respectively, at the DFT/B3LYP and DFT/CAM-B3LYP[48,49] levels, both in the gas phase and in cyclohexane. In our calculations, the standard parametrization ($\alpha = 0.190$, $\beta = 0.460$, $\mu = 0.330$) was used for CAM-B3LYP. The DALTON 2.0 quantum chemistry program[50] was employed using the implementation described in refs 15 and 20. All calculations were carried out with the aug-cc-pVDZ[51] basis set. In the gas-phase calculations, labeled GAS/B3LYP and GAS/CAM-B3LYP in the following, the TD-DFT response equations were solved for the lowest 16 excited electronic states. The calculations in PCM are from now on labeled PCM/B3LYP and PCM/CAM-B3LYP, respectively.

4. RESULTS AND DISCUSSION

4.1. "Vertical-Transition" Spectral Analysis.

4.1.1. B3LYP vs CAM-B3LYP; Gas Phase vs PCM. This section presents and analyzes the OPA and MCD spectra obtained considering only the electronic degrees of freedom, i.e., from vertical transitions between the electronic states and thus

dx.doi.org/10.1021/ct301101h | J. Chem. Theory Comput. 2013, 9, 1557−1567

without taking vibrational states into account. Figure 1 shows the OPA (left, bottom panel) and MCD (left, top panel) spectra of biphenylene calculated at the B3LYP/aug-cc-pVDZ and CAM-B3LYP/aug-cc-pVDZ levels both in the gas phase and in cyclohexane. A Lorentzian line width of 0.1 eV was employed for all excited states in order to broaden the vertical transition lines. The data used to draw the spectra are summarized in Table 1, which reports the vertical excitation energies E^e_{gf} (eV), vertical one-photon absorption intensity reported as $I_{OPA} = |\mu^e_\alpha|^2$ (au), and vertical magnetic circular dichroism intensity reported as $I_{MCD} = -\varepsilon_{\alpha\beta\gamma}\,\mathrm{Im}[\mu^e_\alpha T^{e*}_{\beta\gamma}]$ (au). We also show the corresponding experimental spectra in the right panels of Figure 1. A detailed analysis of the comparison with experiment will be delayed to section 4.1.2.

For our system, CAM-B3LYP yields spectra that are blue-shifted with respect to those predicted by B3LYP. This is consistent with our previously reported results on *R*-(+)-3-methylcyclopentanone[30,52] and *R*-(+)-1,1′-bis(2-naphtol),[53] as well as the results from a benchmark study on an extended set of molecules.[54] All calculations predict five allowed transitions in the spectral region we investigated, but with different intensities and in a different order at different levels of theory. The gas-phase calculations predict different optical responses with respect to the solvated ones, in terms of both OPA and MCD, and the profiles in solvent show a red shift with respect to the vapor phase, as is clearly seen in Figure 1 and Table 1.

As can be seen from Table 1, CAM-B3LYP predicts larger intensities compared to B3LYP for OPA, and a small peak in the short wavelength region (see the left bottom panel in Figure 1, around 52 000 cm^{-1}), which corresponds to the contribution from S14 for the gas phase and S13 in cyclohexane. This absorption is not present at the B3LYP level within the first 16 states, and it actually arises from a contribution from a higher state, for example S22 in cyclohexane. As can be seen from Figure 1, the PCM calculations give similar spectral profiles with respect to the gas-phase predictions but with a red shift of the largest absorption peak. Turning to Table 1, we note that the gas-phase calculations predict respectively the S6 state (B_{1u}, in-plane polarized along the molecular long axis *z*) as the most intense OPA state by B3LYP and the S5 state by CAM-B3LYP, which turns out to be the S4 state in cyclohexane for both functionals; the absorption intensity is enhanced by the dielectric medium, a common feature often observed for PCM at the linear response level.[55] All calculations predict S2 as the second-most intense OPA state; the transition being z polarized, in agreement with the B_{1u} symmetry of the S2 state.

The PCM calculations show a quite different MCD response compared to the gas-phase results, especially for B3LYP, as can be seen from Figure 1. The B3LYP calculations both in the gas phase and with PCM predict a negative MCD signal around 30 000 cm^{-1}, see Figure 1, with the intensity enhanced by the solvent, and this band is assigned to the S2 state. The GAS/B3LYP calculation gives two negative peaks around 40 000 cm^{-1}, which change to a large negative and a small positive signal in the solvent. The data in Table 1 show that the two negative peaks in the gas phase originate from the S4 and S6 states, whereas in the solvent the response in this region arises from a large negative signal for S4 and a large positive response for S5, leading to an overall small positive feature after partial overlap with the response of the S4 state, which is only 0.09 eV lower in energy relative to S5. B3LYP predicts a positive MCD signal for S9 and a negative one for S12, in both the gas phase and solvent. The GAS/CAM-B3LYP MCD spectrum around 45 000 cm^{-1} resembles the PCM/B3LYP spectrum at 40 000 cm^{-1}, in the sense that an analogous cancellation takes place between the strong positive signal (from S6) and the strong negative signal of its neighboring S5 state since these two states are 0.09 eV apart. Also the PCM/CAM-B3LYP shows a large negative and a small positive signal in this region, but in this case the small positive signal is not due to a partial overlap of bands of different sign but originates from the response of the S6 state, 0.32 eV higher in energy than S4, which is the source of the large negative signal. B3LYP predicts a negative signal in the region where the S12−S14 absorbs, both in the gas phase and in cyclohexane, whereas CAM-B3LYP shows a positive signal, slightly shifted toward the blue.

4.1.2. Comparison to Experiment. Experimental OPA in stretched polymer sheets at room temperature shows a weak absorption around 29 000 cm^{-1} and a strong absorption around 41 000 cm^{-1}, both showing a vibrational structure (*vide infra*). The polarization of the experimental spectrum is along the *z* axis, confirming the assignment to states belonging to the B_{1u} irrep (S2 and S4 at the PCM/B3LYP level of theory). Room-temperature experimental MCD spectra in cyclohexane exhibit two structured bands around 28 000−31 000 cm^{-1} and 40 000−41 000 cm^{-1} whose line shape is rather similar to the corresponding OPA bands, whereas it differs noticeably from the OPA above 41 500 cm^{-1}. In the 35 000−38 000 cm^{-1} region, the OPA and MCD show respectively a weak absorption and a weak bisignate signal. All calculations reproduce well the relative position of the two regions of the experimental OPA spectrum and qualitatively the fact that the high-energy band is more intense than the low-energy one, with PCM/B3LYP giving the best agreement with the experiment. B3LYP gives a better description of the peak positions, whereas CAM-B3LYP predicts both peaks blue-shifted relative to the experimental data. For MCD, only PCM/B3LYP correctly reproduces the sign of the MCD signals, whereas GAS/B3LYP could not reproduce the small positive peak centered around 42 000 cm^{-1} in the experimental data. The CAM-B3LYP calculations both in the gas phase and in solvent failed to predict the negative peak in the short wavelength region (around 46 500 cm^{-1}) in the experiment. However, all methods underestimate the differences in the intensities of the weak peak centered at 29 000 cm^{-1} and the strong peak at 41 000 cm^{-1}. In our calculations, the largest ratio between these two peaks is around 3.7 obtained with GAS/CAM-B3LYP, which is much smaller than the factor of about 10 observed in experiment. Moreover, as can be seen from Table 1, the second peak even suffers from a cancellation with the strong positive signal of its neighbor, which further decreases the intensity differences.

The complex polarization propagator (CPP) developed by Norman et al.[56,57] and successfully applied in our previous work[23,58] provides an alternative approach for the calculation of MCD spectra of closed-shell molecules. In the CPP approach, the finite lifetimes of the excited states are taken into account, avoiding in this manner the unphysical divergences appearing in the conventional response functions at the resonances of the molecular system. CPP can therefore be applied to double-check our calculations since it should deliver results identical to the conventional response calculation applied in the present study if there are no nearly degenerate excited states. To perform this comparison, we selected the PCM/B3LYP level of theory since, according to conventional response theory, it provides the best agreement with experimental results. Figure 2

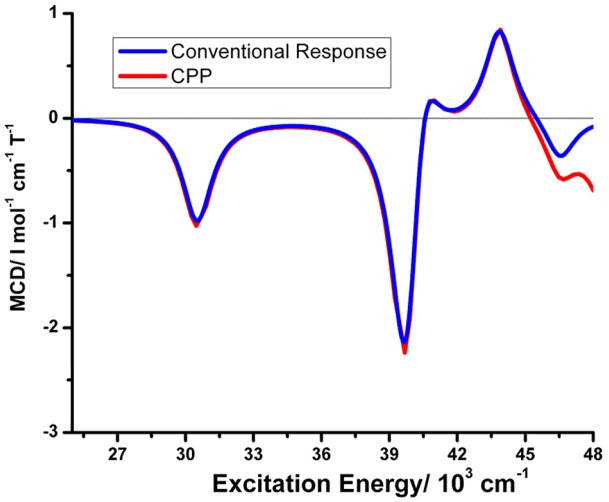

Figure 2. The MCD spectra of biphenylene calculated at the B3LYP/aug-cc-pVDZ level of theory in cyclohexane. A Lorentzian line width of 0.1 eV was employed for the conventional response spectrum (red line). For the CPP spectrum (blue line), the excited-state lifetime broadening is also set to 0.1 eV, and the frequencies have been calculated with a separation of 0.001 hartree.

shows that the CPP predictions agree very well with the conventional response calculations, thus confirming the reliability of our calculated spectra. The divergence of the two spectra in the blue region is due to the fact that we only included up to 16 excited states in the conventional response calculation.

4.2. Vibrationally Resolved One-Photon Absorption. Vibronically resolved OPA spectra have been computed using PCM/B3LYP/aug-cc-pVDZ and are shown in Figure 3.

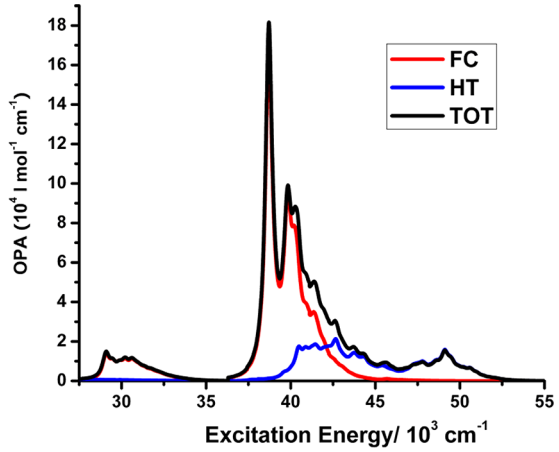

Figure 3. The vibronically resolved OPA spectrum of biphenylene, calculated using PCM/B3LYP/aug-cc-pVDZ.

Although the calculated spectra cover a region of wavelengths encompassing the first 16 excited electronic states, we will focus on the region up to 47 000 cm^{-1} as in the experiment, which corresponds to the 13th excited state in our calculation. It is worth mentioning that the convoluted spectra in the region of the highest computed states, S14–S16 in the present case, might be affected by the neglect of higher states as the algorithm used to determine the excited states does not necessarily ensure that the lowest roots are found. FC, HT, as well as total (TOT = FC + HT) spectra are shown, with a Lorentzian broadening lifetime of 0.03 eV in order to allow the finer details of the vibrational structure to be visible. A qualitative assessment of the relative importance of the FC and HT terms can be made on the basis of an analysis of their contributions to the total intensities for each electronic transition; these can be computed from the analytical sums in eqs 12 and 14 for OPA and MCD, respectively. Similar discussions have been made in earlier studies of electronic circular dichroism[30] and two-photon circular dichroism.[31] The calculated total FC and HT intensities obtained with the PCM/B3LYP approach for both OPA and MCD are given in Tables 1 (FC) and 2 (HT). The convergence of the spectra for each electronic state has been carefully checked, and all the spectra are fully converged. As can be seen from Figure 3, the OPA spectrum in the region of the first two peaks—where the S2 and S4 states absorb—is dominated by FC with rather negligible HT contributions. HT contributions become significant above 40 000 cm^{-1} and arise from the otherwise symmetry-forbidden S6 (A_g symmetry) and S8 (B_{3g} symmetry) states. The HT contributions of S12, S13, and S16 together give rise to the small absorptive peak at the shortest wavelength region of the spectra.

Table 2. Herzberg–Teller (au) OPA and MCD Intensities for the First 16 Excited States of Biphenylene Using PCM/B3LYP/aug-cc-pVDZ[a]

state	sym	E^e_{gf}	I^{HT}_{OPA}	I^{HT}_{MCD}
S1	B_{3g}	3.24	0.2487	−0.5826
S2	B_{1u}	3.79	0.0147	0.1129
S3	B_{2g}	4.77	0.0780	−0.6438
S4	B_{1u}	4.93	0.0263	−0.0587
S5	B_{3u}	5.02	0.2892	−1.5291
S6	A_g	5.08	1.7814	0.0835
S7	A_u	5.20	0.0101	−0.4405
S8	B_{3g}	5.33	1.0955	−1.7613
S9	B_{2u}	5.44	0.0146	1.8443
S10	B_{2g}	5.52	0.0064	−0.2391
S11	B_{1g}	5.59	0.0105	0.3341
S12	B_{2u}	5.77	0.3269	−8.1027
S13	A_g	5.86	0.3150	2.2349
S14	B_{2g}	6.00	0.0572	−1.2309
S15	A_u	6.01	0.0293	0.0597
S16	A_u	6.08	0.5222	−5.8759

[a]Note that the FC total intensities coincide with those given in Table 1. For each state, the irrep it belongs to is indicated.

The experimental OPA spectrum shows pronounced fine structures in the absorption region of the S2 and S4 states, respectively. In order to perform a more detailed comparison with experimental data, in Figure 4 we give both the stick and convoluted (with a Lorentzian broadening lifetime of 0.03 eV) spectra of S2 and S4. The vibrational assignments of the main stick bands are also shown.

The predicted vibrational progressions of the S2 spectrum (upper panel in Figure 4) are in very good agreement with experimental data. The most intense peak is mainly due to the 0–0 transition. The 0–1 transition of mode 6 with a frequency of 398 cm^{-1}, which corresponds to a collective in-plane C–C–C bending of the two phenyl rings (and reproduces a stretching of the rings), is the second-most intense peak, but it probably falls within the 0–0 peak in the experimental spectrum. The experiment shows two peaks shifted toward the blue by roughly

dx.doi.org/10.1021/ct301101h | J. Chem. Theory Comput. 2013, 9, 1557–1567

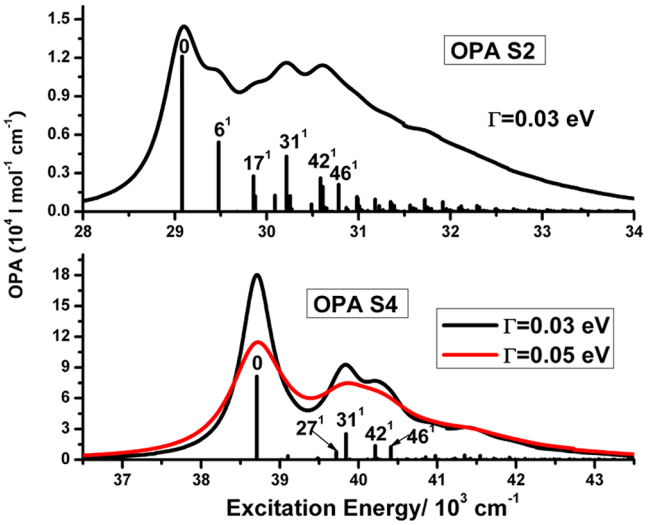

Figure 4. The stick and convoluted (with a Lorentzian broadening lifetime of 0.03 eV) OPA spectra of S2 and S4. The spectrum convoluted with a larger Lorentzian lifetime of 0.05 eV(red line) is also given for S4.

1000−1100 and 1400−1500 cm^{-1}, which upon inspection of Figure 4 can be assigned to the 0−1 transitions of mode 31 with a frequency of 1136 cm^{-1} and of mode 42 with a frequency of 1508 cm^{-1}, respectively. Both modes correspond to the stretching of the middle ring along the molecular main axis, with the latter related to the stretching of the phenyl rings along the short axis as well. The 0−1 transition of modes 17 (with a frequency of 778 cm^{-1} and corresponding to the C−C−C bending of the two phenyl rings) and 46 (with a frequency of 1705 cm^{-1} and corresponding to the C−C stretching of the middle ring) also give significant contributions to the spectrum. As far as the absolute position of the spectrum is concerned, it is worth noticing that in most cases, Duschinsky mixings and changes in the frequencies of the ground and excited states cause a red-shift of the spectrum (on the order of 0.1 eV for medium-sized π-delocalized systems),[59] and it is reasonable to assume that the inclusion of these contributions would further improve the agreement with experimental data.

The convoluted OPA spectrum for the S4 state with a lifetime of 0.03 eV (see the black line in the bottom panel of Figure 4) shows a more pronounced vibrational structure than in the experiment, whereas a very good agreement with the experiment can be obtained with an increased lifetime of 0.05 eV, see the red line. This suggests that S4 has a shorter lifetime than S2. The 0−0 transition is responsible for the strongest stick band, which also produces the strongest peak in the convoluted spectrum. The fundamentals of modes 31, 42, and 46, which give very important contributions to the S2 state, show very large contributions for S4 as well, and they altogether give rise to the second strongest peak in the convoluted spectrum. Mode 27, with a frequency of 1011 cm^{-1} and corresponding to C−H bendings, also gives a notable contribution to the spectrum. The experimental spectrum shows a peak blueshifted from the 0−0 transition by ∼1200 cm^{-1}, and this can be assigned to the fundamental of mode 31. Interestingly, our simulations are able to reproduce the observation that the two peaks at ∼1200 cm^{-1} and ∼1500 cm^{-1} have roughly the same intensity in the S2 spectrum, while the former is dominant in the S4 spectrum. A closer inspection of Figure 4 shows that the relative intensity of the fundamentals of modes 31 and 42 are similar in the two states, making the peak at 1500 cm^{-1} as intense as the peak at 1200 cm^{-1}. In the S2 spectrum, there is a second peak adjacent to the 0−0 band and corresponding to the combination band of modes 6 and 31; this latter peak is not visible in the S4 spectrum because mode 6 is in this case much less displaced.

4.3. Vibrationally Resolved Magnetic Circular Dichroism. In Figure 5, we report the vibrationally resolved MCD spectrum of biphenylene calculated at the PCM/B3LYP/aug-cc-pVDZ level in the spectral region covered by the first 16 electronic excited states. FC, HT, as well as total (TOT = FC +

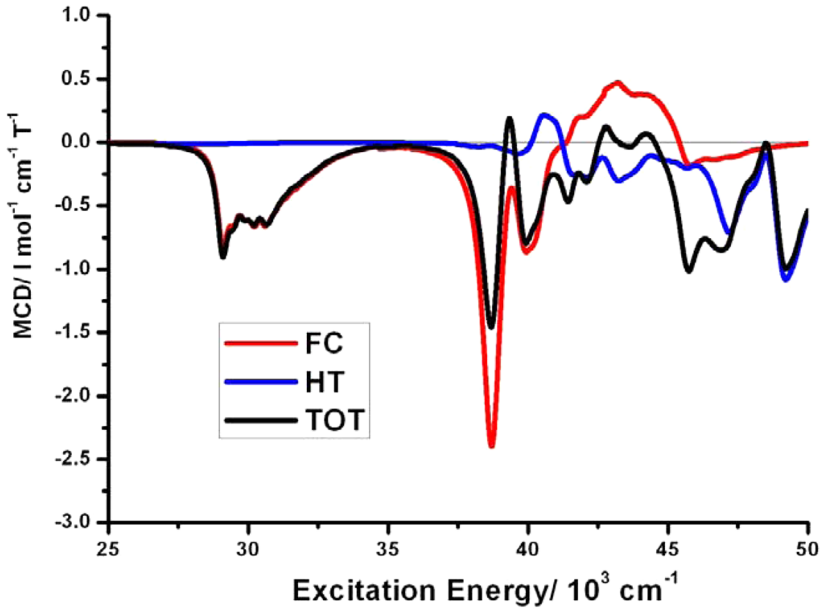

Figure 5. The vibronically resolved MCD spectrum of biphenylene, calculated using PCM/B3LYP/aug-cc-pVDZ, in a spectral region covering the first 16 electronic excited states. FC, HT, as well as total (TOT = FC + HT) spectra are shown. A Lorentzian broadening lifetime of 0.03 eV has been applied for the first two excited states, and a Lorentzian broadening lifetime of 0.05 eV has been applied for the other states.

dx.doi.org/10.1021/ct301101h | J. Chem. Theory Comput. 2013, 9, 1557−1567

HT) spectra are shown. The OPA analysis gives support for convoluting the spectra with a Lorentzian lifetime broadening of 0.03 eV for the first two excited states, but a larger broadening of 0.05 eV for the higher states.

The MCD spectrum computed at the FC level is in fairly nice agreement with experimental data over the entire energy range. Figure 6 analyzes the spectrum in terms of the

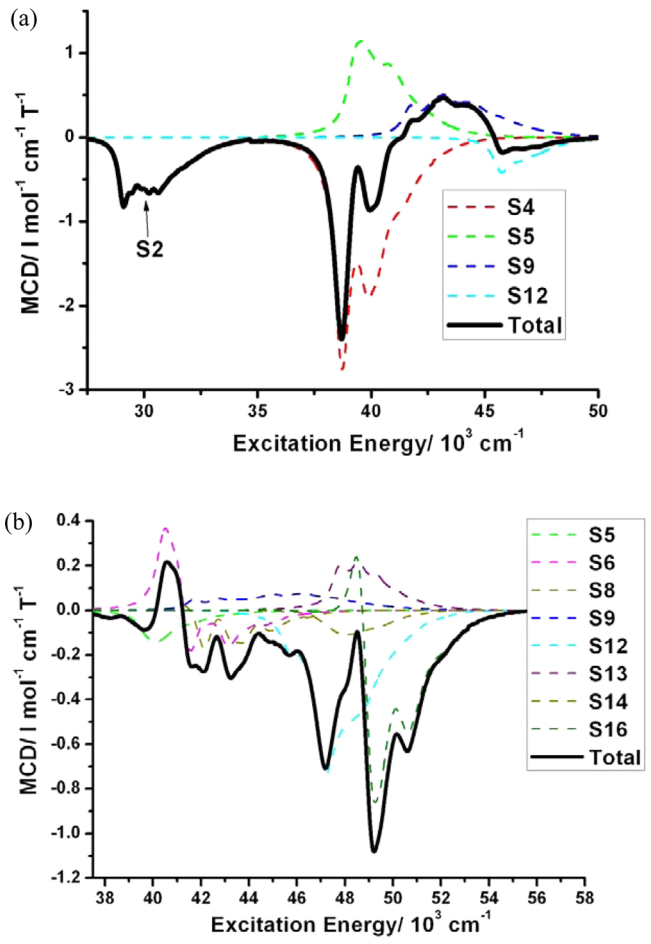

Figure 6. The vibronically resolved MCD spectrum of biphenylene, calculated using PCM/B3LYP/aug-cc-pVDZ, in a spectral region covering the first 16 electronic excited states. FC (see panel a) and HT (see panel b) spectra are shown. A Lorentzian broadening lifetime of 0.03 eV has been applied for the first two excited states, and a Lorentzian broadening lifetime of 0.05 eV has been applied for the other states. The individual contributions from the states contributing the most to the total spectrum are shown in dashed lines.

contributions of the individual vibronically broadened electronic states. In the region up to 35 000 cm^{-1}, a negative signal with a marked vibrational progression is predicted and assigned to the S2 state. Around 40 000 cm^{-1}, a pair of intense negative peaks attributed to a vibrational progression along the S4 state are predicted, while at higher energies the signal turns into a broad and almost structureless positive band arising from the combined effect of the S5 and S9 states. Above 45 000 cm^{-1}, the signal becomes negative again, with the main contribution coming from state S12. As already noted, the high-energy tail of the MCD spectrum might be affected by the finite number of excited states considered.

For the S2 state, the calculated MCD spectrum shows the same vibrational progressions as the OPA spectrum; this is as expected because they both are dominated by FC contributions (leading to the same vibrational structure) and because the MCD arises from the isolated S2 state. This is also approximately observed in the experiments. In fact, as was the case for OPA, the main vibrational peak is shifted toward the blue with respect to the 0−0 transition by ∼1400 cm^{-1} and shows a red-shifted shoulder separated by ∼1200 cm^{-1} from the 0−0 peak. Minor differences appear in the experimental OPA and MCD spectra: specifically, the former seems more resolved and with fewer vibrational peaks than the latter, especially in the energy region between the 0−0 and the second strongest peak. Our level of theory does not allow us to rationalize these finer details, but it can be speculated that the observed differences are due to the different experimental conditions, so that the polymer-stretched sheets cause a larger broadening than cyclohexane.

The ratio of the (absolute) intensities of the doublet at 40 000 and 39 000 cm^{-1} (which in the experiment respectively corresponds to those at 41 000 and 40 000 cm^{-1}) is smaller than what is seen in OPA, in agreement with experimental data. Figure 6 allows attribution of the de-enhancement of the higher-energy component of the doublet to the partial cancellation between an excited vibrational peak of S4 (see the red dashed line in Figure 6) and the 0−0 transition of S5 (see the green dashed line in Figure 6).

Figure 5 indicates that the inclusion of the HT contribution worsens the agreement with experiment notably. Analysis of FC and HT contributions to the total intensities, given in Tables 1 and 2, respectively, provides a first indication of their relative relevance in determining the MCD line shape. However, we recall that MCD spectra can involve delicate cancellations of positive and negative contributions (see for instance Table S1 in the SI), so that the HT contribution behaves in a far more complex way than in the corresponding absorption spectra. Therefore, the actual relevance of the HT effect for the spectral profile may be difficult to estimate from an analysis of the total intensities only. This is actually also the case for OPA (but less dramatic) due to the possible occurrences of FC/HT interferences that modulate the band shape but not the total intensity.[60] For a better understanding of the spectra, in Figure 6 we plot both FC and HT contributions from the most intense states. As can be seen from the figure, in the region of S1, the FC mechanism dominates the spectrum, and there are only negligible HT contributions. These latter become significant above 35 000 cm^{-1} and modulate the TOT spectra signficantly.

Equation 14 shows that the HT total intensity of MCD I_{MCD}^{HT} of a given electronic state arises from the sum of the contributions of the individual modes. For each excited state showing a remarkable HT effect, Table S1 in the SI reports the three modes that give the strongest contributions. It can be noted that these modes belong to non-totally symmetric irreps with the exception of the mode giving the third (in order of importance) contribution to I_{MCD}^{HT} of the S5 state. Since only totally symmetric modes can contribute to the non-Condon mechanism connected to the variation of $\omega_k - \omega_g$ with the nuclear coordinates (eqs 9, 10), proposed by Zgierski,[29] we conclude that this latter is of minor importance for the MCD of biphenylene. A very complicated picture arises from the analysis of the data in Table S1. In fact, for many of the investigated states, several modes introduce very strong contributions of different sign, so that the final I_{MCD}^{HT} value is the result of a near-cancellation of opposite contributions. In such a situation, it is reasonable to expect that even small computational inaccuracies

might cause significant variations in the predicted spectra, so that the HT contributions to MCD spectral shapes must be interpreted with caution.

We recall that the HT theory of intensity borrowing was derived using first-order perturbation theory assuming that the vibronic wave functions are not affected by vibronic coupling. It can therefore only be safely applied to describe the intensity borrowing of weak states that are well separated in energy from the strong states that lend intensity. When the intensity-borrowing mechanism is straightforwardly applied to states featuring strong FC signals, the HT treatment can lead to unphysical effects, described in some detail for OPA in ref 58 and for ECD in ref 61; as an example the total OPA intensity of strong states (that should lend intensity) is predicted to be increased by the HT effect and the same happens for the overall intensity of the interacting states. In contrast, the overall intensity should be constant on the basis of a rigorous variational treatment. When considering the case of biphenylene, we note that (i) several electronic states fall in the region of the spectrum characterized by strong HT effects (the energy gap between the S5 and S12 states is only 0.7 eV), so that interstate mixings are actually likely, and (ii) comparison of the FC and HT contributions in Figure 6 highlights that the S_5, S_9, and S_{12} states, which show major contributions to the FC spectrum, also contribute notably to the HT effects. According to the above discussion, this is a situation in which it is likely that the HT treatment is not fully reliable.

A thorough analysis of the possible occurrence of nonadiabatic couplings among the states involved in the MCD response is outside the scope of this work. However, we have performed a preliminary exploration of the excited-state minima and normal modes of the S4 and S6 states, performed adopting a more computationally convenient basis set, and reported in detail in the SI, that indicates that in the D_{2h} symmetry, the S4 state features a strong imaginary frequency (i900 cm^{-1}) along a b_{1u} mode. Distortion along this mode leads to a global minimum having C_{2v} symmetry, where both the S4 and S6 states belong to the A_1 irrep and clearly mix, as indicated by the interchange of OPA intensity. Such a situation strongly suggests the existence of significant nonadiabatic couplings that potentially make the MCD spectral line shape different from the OPA one and which cannot be treated within HT theory.

We close this section noting that in our calculated MCD spectrum there is no visible signal at about 35 000−38 000 cm^{-1} where the MCD experiment seems to show a bisignate signal. Actually, the S3 state lies in this energy region, and from Table 2 it can be seen that at the HT level it acquires some negative intensity but it is too weak to appear in the spectra. It is plausible that the polymer may interact with the biphenylene in such a manner that the S3 state becomes symmetry-allowed, at least to the extent that it can also induce interactions with the S4 state and increase the MCD rotational strength in combination with the HT contribution.

5. CONCLUSIONS

We have applied a density functional theory approach to study the OPA and MCD spectral properties of biphenylene, in which we have chosen PCM to account for the effect from the surrounding environment and VG vibronic models to introduce the vibrational fine structures. A detailed comparison with experimental spectra has been performed. We have shown that better agreement with experimental data is obtained when including solvent effects. In the framework of the adiabatic approximation, different vibronic mechanisms of the Franck−Condon and Herzberg−Teller types have been analyzed in detail. The calculations indicate that caution should be exercised when performing HT calculations on systems such as biphenylene, which has close-lying electronic states that may induce nonadiabatic vibronic couplings. A preliminary discussion of these effects has been presented in the paper.

■ ASSOCIATED CONTENT

Supporting Information

The modes giving rise to the largest Herzberg−Teller effects on the MCD spectrum are listed in Table S1. The possible occurrence of nonadiabatic effects in the MCD spectrum of biphenylene has been investigated in section S1 and Table S2. This material is available free of charge via the Internet at http://pubs.acs.org

■ AUTHOR INFORMATION

Corresponding Author

*E-mail: zhaoxian@sdu.edu.cn; fabrizio.santoro@iccom.cnr.it.

Notes

The authors declare no competing financial interest.

■ ACKNOWLEDGMENTS

This work has been supported by the Research Council of Norway through a Center of Excellence Grant (Grant No. 179568/V30) and a research grant (Grant No. 191251/V30). A grant of computer time from the program for Norwegian Supercomputing is gratefully acknowledged. N.L. acknowledges the support from the National Nature Science Foundation of China (Grant No. 21003085) and Independent Innovation Foundation of Shandong University (2009HW002). F.S. acknowledges support from MIUR (FIRB "Futuro in Ricerca" RBFR10Y5VW).

■ REFERENCES

(1) Nakanishi, K.; Berova, N.; Woody, R. W. *Circular Dichroism: Principles and Applications*; VCH: New York, 1994.

(2) Buckingham, A. D.; Stephens, P. J. Magnetic Optical Activity. *Annu. Rev. Phys. Chem.* **1966**, *17*, 399.

(3) Stephens, P. J. Theory of Magnetic Circular Dichroism. *J. Chem. Phys.* **1970**, *52*, 3489.

(4) Stephens, P. J. Magnetic Circular-Dichroism. *Annu. Rev. Phys. Chem.* **1974**, *25*, 201.

(5) Kjærgaard, T.; Coriani, S.; Ruud, K. Ab initio calculation of magnetic circular dichroism. *Wires Comput. Mol. Sci.* **2012**, *2*, 443.

(6) Helgaker, T.; Coriani, S.; Jørgensen, P.; Kristensen, K.; Olsen, J.; Ruud, K. Recent Advances in Wave Function-Based Methods of Molecular-Property Calculations. *Chem. Rev.* **2012**, *112*, 543.

(7) Barron, L. D. *Molecular Light Scattering and Optical Activity*, 2nd ed.; Cambridge University Press: Cambridge, U. K., 2004.

(8) Neese, F.; Solomon, E. I. MCD C-term signs, saturation behavior, and determination of band polarizations in randomly oriented systems with spin $S \geq 1/2$. Applications to $S = 1/2$ and $S = 5/2$. *Inorg. Chem.* **1999**, *38*, 1847.

(9) Mason, W. R. *A Practical Guide to Magnetic Circular Dichroism Spectroscopy*; Wiley-Interscience: New York, 2007.

(10) Fleischhauer, J.; Howeler, U.; Spanget-Larsen, J.; Raabe, G.; Michl, J. Magnetic circular dichroism of nonaromatic cyclic pi-electron systems. 5. Biphenylene and its aza analogues. *J. Phys. Chem. A* **2004**, *108*, 3225.

(11) Jorgensen, N. H.; Pedersen, P. B.; Thulstrup, E. W.; Michl, J. Semi-Empirical Pi-Electron Models for the Calculation of Mcd B-Terms for Systems with Approximate Alternant Pairing Symmetry - Mcd of Biphenylene. *Int. J. Quantum Chem.* **1978**, *S12*, 419.

(12) Seamans, L.; Moscowit, A. Theorem Useful for Interpretation of Magnetic Circular-Dichroism Spectra. *J. Chem. Phys.* **1972**, *56*, 1099.
(13) Olsen, J.; Jørgensen, P. Linear and nonlinear response functions for an exact state and for an MCSCF state. *J. Chem. Phys.* **1985**, *82*, 3235.
(14) Salek, P.; Vahtras, O.; Helgaker, T.; Ågren, H. Density-functional theory of linear and nonlinear time-dependent molecular properties. *J. Chem. Phys.* **2002**, *117*, 9630.
(15) Coriani, S.; Jørgensen, P.; Rizzo, A.; Ruud, K.; Olsen, J. *Ab initio* determinations of magnetic circular dichroism. *Chem. Phys. Lett.* **2000**, *300*, 61.
(16) Caricato, M.; Mennucci, B.; Tomasi, J.; Ingrosso, F.; Cammi, R.; Corni, S.; Scalmani, G. Formation and relaxation of excited states in solution: A new time dependent polarizable continuum model based on time dependent density functional theory. *J. Chem. Phys.* **2006**, *124*, 124520.
(17) Miertus, S.; Scrocco, E.; Tomasi, J. Electrostatic Interaction of a Solute with a Continuum - a Direct Utilization of Abinitio Molecular Potentials for the Prevision of Solvent Effects. *Chem. Phys.* **1981**, *55*, 117.
(18) Tomasi, J.; Persico, M. Molecular-Interactions in Solution - an Overview of Methods Based on Continuous Distributions of the Solvent. *Chem. Rev.* **1994**, *94*, 2027.
(19) Tomasi, J.; Mennucci, B.; Cammi, R. Quantum mechanical continuum solvation models. *Chem. Rev.* **2005**, *105*, 2999.
(20) Solheim, H.; Frediani, L.; Ruud, K.; Coriani, S. An IEF-PCM study of solvent effects on the Faraday B term of MCD. *Theor. Chem. Acc.* **2008**, *119*, 231.
(21) Fischer, G. *Vibronic Coupling: the Interaction between the Electronic and Nuclear Motions*; Academic Press: London, 1984.
(22) Califano, S. *Vibrational States*; Wiley: London, 1976.
(23) Solheim, H.; Ruud, K.; Coriani, S.; Norman, P. The A and B terms of magnetic circular dichroism revisited. *J. Phys. Chem. A* **2008**, *112*, 9615.
(24) (a) Craig, D. P.; Thirunamachandran, T. *Molecular Quantum Electrodynamics: An Introduction to Radiation-Molecule Interactions*; Academic: London, 1984; pp xi, 324. (b) Tinoco, I. 2-Photon Circular-Dichroism. *J. Chem. Phys.* **1975**, *62* (3), 1006.
(25) Rizzo, A.; Coriani, S.; Ruud. K. *Computational Strategies for Spectroscopy*; Barone, V., Ed.; Wiley and Sons: Hoboken, NJ, 2012; pp 77−135.
(26) Sterzel, M.; Andrzejak, M.; Pawlikowski, M. T.; Gawroński, J. Absorption and magnetic circular dichroism (MCD) studies of 1,4,5,8-naphthalenetetracarboxy diimides in terms of CASSCF method and FC theory. *Chem. Phys.* **2004**, *300*, 93.
(27) Zazakowny, P.; Pawlikowski, M. T.; Sterzel, M. The vibronic structures of absorption and magnetic circular dichroism (MCD) in the low energy 1(1)B(2u) and 1(1)B(3u) states of 1,4,5,8-naphthalenetetracarboxy dianhydride. The analysis in terms of DFT and CASSCF methods. *Chem. Phys. Lett.* **2009**, *472*, 55.
(28) Ganyushin, D.; Neese, F. First-principles calculations of magnetic circular dichroism spectra. *J. Chem. Phys.* **2008**, *128*, 114117.
(29) Zgierski, M. Z. Vibronic structure of MCD spectra. I. Non-Condon effects in molecules with nondegenerate electronic states. *J. Chem. Phys.* **1985**, *83*, 2170.
(30) Lin, N.; Santoro, F.; Zhao, X.; Rizzo, A.; Barone, V. Vibronically Resolved Electronic Circular Dichroism Spectra of (R)-(+)-3-Methylcyclopentanone: A Theoretical Study. *J. Phys. Chem. A* **2008**, *112*, 12401.
(31) Lin, N.; Santoro, F.; Rizzo, A.; Luo, Y.; Zhao, X.; Barone, V. Theory for Vibrationally Resolved Two-Photon Circular Dichroism Spectra. Application to (R)-(+)-3-Methylcyclopentanone. *J. Phys. Chem. A* **2009**, *113*, 4198.
(32) Macak, P.; Luo, Y.; Ågren, H. Simulations of vibronic profiles in two-photon absorption. *Chem. Phys. Lett.* **2000**, *330*, 447.
(33) Macak, P.; Luo, Y.; Norman, P.; Ågren, H. Electronic and vibronic contributions to two-photon absorption of molecules with multi-branched structures. *J. Chem. Phys.* **2000**, *113*, 7055.
(34) Minaev, B.; Wang, Y. H.; Wang, C. K.; Luo, Y.; Ågren, H. Density functional theory study of vibronic structure of the first absorption Q(x) band in free-base porphin. *Spectrochim. Acta, Part A* **2006**, *65*, 308.
(35) Santoro, F. *FCClasses*, a Fortran 77 code available at http://village.pi.iccom.cnr.it (accessed Jan 26, 2013).
(36) Gierschner, J.; Mack, H. G.; Egelhaaf, H. J.; Schweizer, S.; Doser, B.; Oelkrug, D. Optical spectra of oligothiophenes: vibronic states, torsional motions, and solvent shifts. *Synth. Met.* **2003**, *138*, 311.
(37) Gierschner, J.; Mack, H. G.; Luer, L.; Oelkrug, D. Fluorescence and absorption spectra of oligophenylenevinylenes: Vibronic coupling, band shapes, and solvatochromism. *J. Chem. Phys.* **2002**, *116*, 8596.
(38) Lin, N.; Zhao, X.; Rizzo, A.; Luo, Y. Vibronic induced one- and two-photon absorption in a charge-transfer stilbene derivate. *J. Chem. Phys.* **2007**, *126*, 244509.
(39) Lin, N.; Luo, Y.; Santoro, F.; Zhao, X.; Rizzo, A. Vibronically-induced change in the chiral response of molecules revealed by electronic circular dichroism spectroscopy. *Chem. Phys. Lett.* **2008**, *464*, 144.
(40) Pritchard, B.; Autschbach, J. Calculation of the Vibrationally Resolved, Circularly Polarized Luminescence of d-Camphorquinone and (S,S)-trans-β-Hydrindanone. *Chem. Phys. Chem.* **2010**, *11*, 2409.
(41) Mort, B. C.; Autschbach, J. Vibrational Corrections to Magneto-Optical Rotation: A Computational Study. *J. Phys. Chem. A* **2007**, *111*, 5563.
(42) Frisch, M. J.; Trucks, G. W.; Schlegel, H. B.; Scuseria, G. E.; Robb, M. A.; Cheeseman, J. R.; Scalmani, G.; Barone, V.; Mennucci, B.; Petersson, G. A.; Nakatsuji, H.; Caricato, M.; Li, X.; Hratchian, H. P.; Izmaylov, A. F.; Bloino, J.; Zheng, G.; Sonnenberg, J. L.; Hada, M.; Ehara, M. T., K.; Fukuda, R.; Hasegawa, J.; Ishida, M.; Nakajima, T.; Honda, Y.; Kitao, O.; Nakai, H.; Vreven, T.; Montgomery, J. A., Jr.; Peralta, J. E.; Ogliaro, F.; Bearpark, M.; Heyd, J. J.; Brothers, E.; Kudin, K. N.; Staroverov, V. N.; Kobayashi, R.; Normand, J.; Raghavachari, K.; Rendell, A.; Burant, J. C.; Iyengar, S. S.; Tomasi, J.; Cossi, M.; Rega, N.; Millam, N. J.; Klene, M.; Knox, J. E.; Cross, J. B.; Bakken, V.; Adamo, C.; Jaramillo, J.; Gomperts, R.; Stratmann, R. E.; Yazyev, O.; Austin, A. J.; Cammi, R.; Pomelli, C.; Ochterski, J. W.; Martin, R. L.; Morokuma, K.; Zakrzewski, V. G.; Voth, G. A.; Salvador, P.; Dannenberg, J. J.; Dapprich, S.; Daniels, A. D.; Farkas, Ö.; Foresman, J. B.; Ortiz, J. V.; Cioslowski, J.; Fox, D. J. *Gaussian 09*, revision A.02; Gaussian, Inc.: Wallingford, CT, 2009.
(43) Becke, A. D. Density-Functional Exchange-Energy Approximation with Correct Asymptotic-Behavior. *Phys. Rev. A* **1988**, *38*, 3098.
(44) Becke, A. D. Density-Functional Thermochemistry. 3. The Role of Exact Exchange. *J. Chem. Phys.* **1993**, *98*, 5648.
(45) Lee, C. T.; Yang, W. T.; Parr, R. G. Development of the Colle-Salvetti Correlation-Energy Formula into a Functional of the Electron-Density. *Phys. Rev. B* **1988**, *37*, 785.
(46) Becke, A. D. A new mixing of Hartree-Fock and local density-functional theories. *J. Chem. Phys.* **1993**, *98*, 1372.
(47) Stephens, P. J.; Devlin, F. J.; Chabalowski, C. F.; Frisch, M. J. *Ab Initio* Calculation of Vibrational Absorption and Circular Dichroism Spectra Using Density Functional Force Fields. *J. Phys. Chem.* **1994**, *98*, 11623.
(48) Yanai, T.; Tew, D. P.; Handy, N. C. A new hybrid exchange-correlation functional using the Coulomb-attenuating method (CAM-B3LYP). *Chem. Phys. Lett.* **2004**, *393*, 51.
(49) Peach, M. J. G.; Helgaker, T.; Salek, P.; Keal, T. W.; Lutnaes, O. B.; Tozer, D. J.; Handy, N. C. Assessment of a Coulomb-attenuated exchange-correlation energy functional. *Phys. Chem. Chem. Phys.* **2006**, *8*, 558.
(50) *DALTON*, a molecular electronic structure program, Release 2.0, see http://www.kjemi.uio.no/software/dalton/dalton.html (accessed Jan 26, 2013).
(51) Dunning, T. H. Gaussian-Basis Sets for Use in Correlated Molecular Calculations 0.1. The Atoms Boron through Neon and Hydrogen. *J. Chem. Phys.* **1989**, *90*, 1007.

(52) Rizzo, A.; Lin, N.; Ruud, K. Ab initio study of the one- and two-photon circular dichroism of R-(+)-3-methyl-cyclopentanone. *J. Chem. Phys.* **2008**, *128*, 164312.
(53) Lin, N.; Santoro, F.; Zhao, X.; Toro, C.; De Boni, L.; Hernandez, F. E.; Rizzo, A. Computational Challenges in Simulating and Analyzing Experimental Linear and Nonlinear Circular Dichroism Spectra. R-(+)-1,1 '-Bis(2-naphthol) as a Prototype Case. *J. Phys. Chem. B* **2011**, *115*, 811.
(54) Jacquemin, D.; Wathelet, V.; Perpète, E. A.; Adamo, C. Extensive TD-DFT Benchmark: Singlet-Excited States of Organic Molecules. *J. Chem. Theory Comput.* **2009**, *5*, 2420.
(55) Mennucci, B. Time dependent solvation: a new frontier for quantum mechanical continuum models. *Theor. Chem. Acc.* **2006**, *116*, 31.
(56) Norman, P.; Bishop, D. M.; Jensen, H. J. A.; Oddershede, J. Nonlinear response theory with relaxation: The first-order hyperpolarizability. *J. Chem. Phys.* **2005**, *123*, 194103.
(57) Norman, P.; Bishop, D. M.; Jensen, H. J. A.; Oddershede, J. Near-resonant absorption in the time-dependent self-consistent field and multiconfigurational self-consistent field approximations. *J. Chem. Phys.* **2001**, *115*, 10323.
(58) Solheim, H.; Ruud, K.; Coriani, S.; Norman, P. Complex polarization propagator calculations of magnetic circular dichroism spectra. *J. Chem. Phys.* **2008**, *128*, 094103.
(59) Avila, F.; Santoro, F. Comparison of vertical and adiabatic harmonic approaches for the calculation of the vibrational structure of electronic spectra. *Phys. Chem. Chem. Phys.* **2012**, *14*, 13549.
(60) Santoro, F.; Improta, R.; Lami, A.; Bloino, J.; Barone, V. Effective method for the computation of optical spectra of large molecules at finite temperature including the Duschinsky and Herzberg-Teller effect: the Qx band of porphyrin as a case study. *J. Chem. Phys.* **2008**, *128*, 224311.
(61) Lin, N.; Solheim, H.; Ruud, K.; Nooijen, M.; Santoro, F.; Zhao, X.; Kwit, M.; Skowronek, P. Vibrationally resolved circular dichroism spectra of a molecule with isotopically engendered chirality. *Phys. Chem. Chem. Phys.* **2012**, *14*, 3669.